Effect of Annealing on Defect Formations in Zno Nanoparticles

Himani Bhoi and Sudhish Kumar

Magnetism Laboratory, Department of Physics, Mohanlal Sukhadia University, Udaipur, Rajasthan, India.

[a] phd_hbhoi@mlsu.ac.in
[b] skphy@mlsu.ac.in

Abstract

This study reports on the effect of annealing on the structural, defect formation and optical characteristics of ZnO nanoparticles (NPs) synthesized via self-combustion reactions. For investigating the effect of annealing, one part of as-synthesized ZnO NPs was kept as such and other two parts were annealed at 450 ºC & 700 ºC (hereafter referred as ZCA, ZCA450 and ZCA700) for six hours in ambient environment. Rietveld refinement of XRD patterns approved phase pure formation of ZCA, ZCA450 & ZCA700 in the Wurtzite type hexagonal symmetry along with a monotonic increment in the unit cell volume and mean crystallite size with annealing temperature (AT). In the same line, observation of three characteristic Raman modes ($2E_{2H}$-$2E_{2L}$, E_2 (high) and E_1 (LO)) validated hexagonal symmetry of these ZnO NPs. Blue shifting in the E_2 (high) and E_1 (LO) modes and red shifting in the $2E_{2H}$-$2E_{2L}$ mode and, ESR analysis corroborated formation of oxygen and zinc vacancies in these ZnO NPs along with annihilation of surface defects with AT. UV-Vis-NIR data exhibited considerable absorption of light below 500 nm by these ZnO NPs with a maximum noted in the blue color region. The obtained band gap E_g = 2.74 eV for ZCA NPs is found to be higher than ZCA450 (E_g = 2.50 eV) and ZCA700 (E_g = 2.68 eV). Notably, the obtained E_g for these ZnO NPs are considerably lower than the reported values in literature. These ZnO NPs seems to be useful for making UV & blue light protection layers and UV absorbers for sunscreen lotion etc.

Keywords: Annealing temperature, optical band gap energy, defects.
Received 28 January 2025; First Review 21 February 2025; Accepted 23 February 2025

*** Address of correspondence**
Himani Bhoi
Department of Physics, Mohanlal Sukhadia University, Udaipur, Rajasthan, India.

Email: phd_hbhoi@mlsu.ac.in

How to cite this article
Himani Bhoi and Sudhish Kumar, Effect of annealing on defect formations in ZnO nanoparticles, J. Cond. Matt. 2024; 02 (02): 94-98.

Available from:
https://doi.org/10.61343/jcm.v2i02.78

Introduction

Nanosized ZnO is a notable wide band semiconducting material with E_g = 3.37 eV and high binding energy (60 meV). ZnO NPs finds substantial applications in the field of chemical, optical and spintronic engineering, etc. It is known for tunable optical and magnetic properties, good thermal and chemical stability, and good biocompatibility. ZnO NPs are being extensively utilized in optoelectronics, LEDs, cosmetics, and biomedical fields like antimicrobial and anticancer treatments [1-2]. Defects, particularly oxygen vacancies in ZnO lattice greatly influence its characteristics and effectiveness [3]. Controlling defects in ZnO along with stoichiometry of oxygen ions and morphology of NPs is essential for better response but demands clear-cut understandings. This study presents augmenting effort on the influence of annealing temperature on the structural & optical properties, and defect formations in ZnO NPs synthesized via self-combustion reactions.

Method

For the synthesis of ZnO NPs, zinc nitrate hexahydrate was used as a precursor and citric acid as a reducing agent, along with few drops of NH_4OH to adjust the pH [4-5]. Stoichiometric amounts of $Zn(NO_3)_2{\cdot}6H_2O$ and $C_6H_8O_7{\cdot}H_2O$ in a 1:1 molar ratio were dissolved in water, combined, and stirred at 50 ºC. NH_4OH was added drop wise to raise the pH to 11. Continuous stirring led to gel formation, which was further heated for initiating combustion reactions and formation of sample desired yield as loose lumps, which were ground into a powder. Synthesis protocol of ZnO NPs is presented in Figure 1. Sample yield was divided into three parts: one part was kept as-synthesized (ZCA), and the other two parts were annealed at 450 ºC (ZCA450) and 700 ºC (ZCA700). X-ray-diffraction (XRD) data were recorded in 20º - 90º range of 2θ (step size = 0.02º) on a RIGAKU ULTIMA-IV. The XRD data were refined using FullProf software. Raman spectrums were recorded on a Horiba JY HR-800 spectrometer using an excitation wavelength of 473 nm. Optical absorption spectrums were recorded in the range of 200-800 nm on the Shimadzu UV-1780 UV-Vis spectrophotometer. ESR data were acquired in X-band (with microwave frequency of ~9.44GHz) on a JEOL Japan made JES-FA200 ESR Spectrometer.

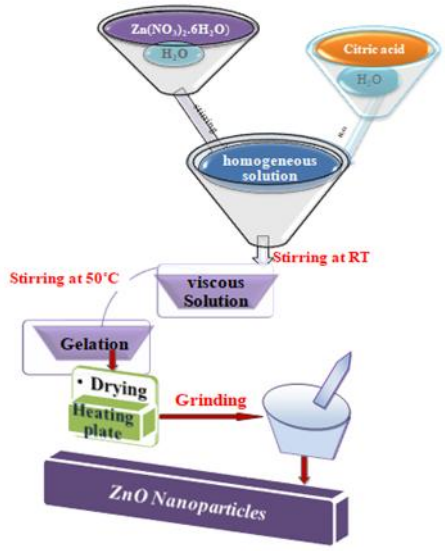

Figure 1: Synthesis protocol of ZnO NPs.

Discussion

The indexed XRD patterns of ZCA, ZCA450, and ZCA700 NPs shown in Figure 2, matched well with the Wurtzite type hexagonal structure (JCPDS 36-1451) with no sign of impurity. The refined hexagonal lattice parameters matched well with the literature (see table 1) [6-7].

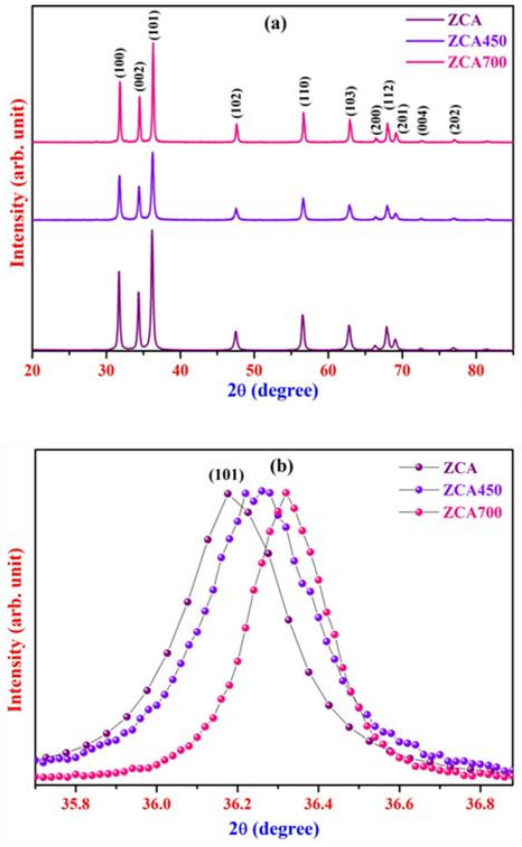

Figure 2: (a) Indexed XRD patterns and (b) shifting in the most prominent (101) XRD peak toward higher 2θ side with AT for ZCA, ZCA450, ZCA700 NPs.

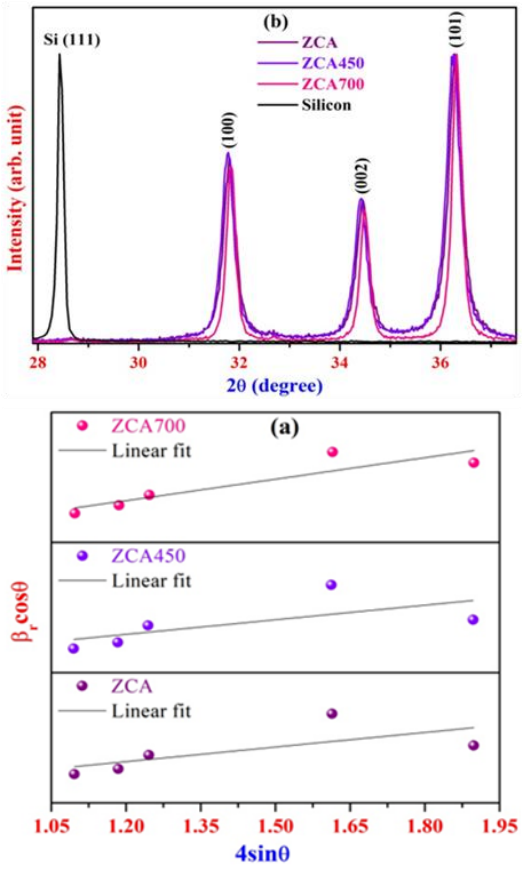

Figure 3: (a) W-H plots and (b) Broadening in the well resolved & intense XRD peaks of ZCA, ZCA450 and ZCA700 NPs compared to standard Silicon's (111) peak in the same region of 2θ.

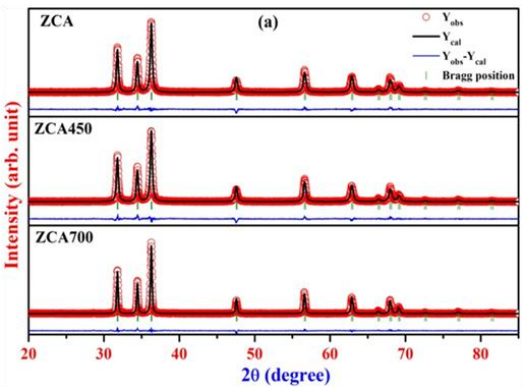

Figure 4: Rietveld refined XRD data of (a) ZCA, ZCA450 and ZCA700 NPs.

As AT increases, the Bragg peaks become sharper and narrower, indicating improvement in the crystallinity. Enhanced peak intensity also reflects this improvement as evident in Figure 2(a). Additionally, the (101) Bragg peak shifts to a higher 2θ side with increasing AT, which is likely due to changes in the stress in ZnO NPs [8]. The mean crystallite size (D) and strain (ε) of ZCA, ZCA450, and ZCA700 NPs (see Figure 3(a)) were deduced using Scherrer's and W-H plot analysis [9], and the results are listed in Table 1. Initially, D does not change much from 35

nm to 36 nm, when annealed at 450°C but annealing at 700°C led to significant enhancement in D to ~59 nm, as reflected in the line broadening shown in Fig. 3(b). Scherrer's method underestimates D but showed the similar trend with W-H method. The microstrain (ε) decreases with AT and thus, indicating tensile stress in these ZnO NPs [10].

Table 1: Crystallographical parameters and agreement factors for ZCA, ZCA450 and ZCA700 NPs

Sample		ZCA	ZCA450	ZCA700
Hexagonal lattice constants (Å)	a = b	3.2494 (3)	3.2495 (3)	3.2500 (3)
	c	5.2071 (5)	5.2077 (5)	5.2062 (4)
Atomic packing fraction (c/a)		1.6025	1.6026	1.6019
Volume (Å^3)		47.615(01)	47.621(01)	47.624(7)
Oxygen's positional Parameter (z)		0.3818	0.3810	0.3823
D ± 5 (nm)	Scherrer method	20	21	30
	W-H plot method	35	36	59
ε×10^{-3}		1.70	1.68	1.38
Density (g/cm^3)		5.676	5.675	5.675
R_{Bragg}		3.47	3.28	2.79
R_f		2.91	2.60	2.45
R_P		9.03	9.10	8.40
R_{wp}		12.9	12.8	13.0
R_{exp}		9.93	9.41	9.58
χ^2		1.69	1.86	1.84

XRD patterns of all samples were refined in the $P6_3mc$ space group (No. 186, Z=2). Nicely fitted XRD profiles are demonstrated in Figure 4. In the refinement, Wyckoff positions were set at 2b (1/3, 2/3, 0) and 2b (1/3, 2/3, z) for Zn and oxygen atoms respectively. According to the crystallography of ZnO only the z coordinate of oxygen is the refinable parameter. Good agreement factors, nice profile fittings and successful indexing of Bragg peaks validated phase pure ZnO NPs crystallizing in the Wurtzite-type hexagonal structure (see table 1). Table 1 also shows that annealing does not alter the hexagonal symmetry of ZnO, though the unit cell volume increases with AT. The refined parameters closely align with each other and also matched well the literature [10].

Raman spectrums of ZCA450 and ZCA700 samples are shown in Figure 5, notably no Raman active modes were observed for ZCA. Positions and classification of observed Raman active modes are presented in table 2. Three characteristic Raman modes corresponding to the Wurtzite type hexagonal symmetry of ZnO are observed. The most intense mode at 438.10 cm^{-1} (ZCA450) and 439.56 cm^{-1} (ZCA700) corresponds to the E_2 (high) mode, while the weak mode at 582.63 cm^{-1} (ZCA450) and 583.87 cm^{-1} (ZCA700) is associated with E_1 (LO) vibrations [11]. Both E_2 (high) and E_1 (LO) modes blue shifted in ZCA700, which is likely due to increased crystallite size, while the weak mode at 346.49 cm^{-1} (ZCA450) is red shifted to 331.67 cm^{-1} in ZCA700. Raman results are in line with the XRD analysis.

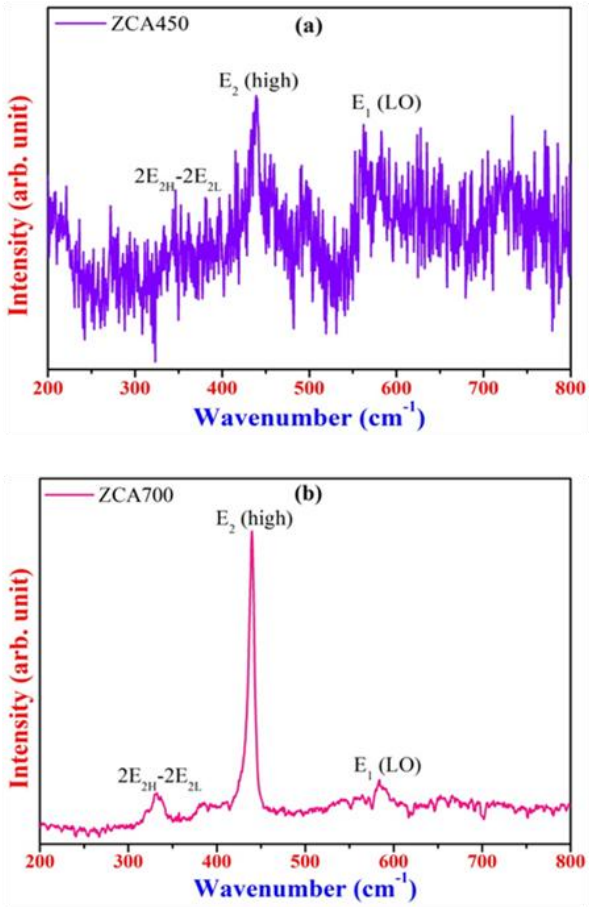

Figure 5. Raman spectrums of (a) ZCA450 and (b) ZCA700.

UV-VIS-NIR absorbance spectrums shown in Figure 6 (a) demonstrate significant light absorption by these ZnO NPs with characteristic maxima at ~376, 378 and 377 nm for ZCA, ZCA450 and ZCA700 NPs, respectively. Further, photo-absorption is increased in ZCA450 NPs compared to the as synthesized ZCA NPs, while it is slightly decreased in ZCA700 NPs. The band gap (E_g) were estimated using Tauc's plots [9,12]. Tauc's plots of ZCA, ZCA450 and ZCA700 NPs are presented in Fig. 6 (b) and estimated E_g values are given in table 2. The E_g = 2.74 eV for as synthesized ZCA is higher than ZCA450 (E_g = 2.50 eV) and ZCA700 (E_g = 2.68 eV). Overall these values of E_g are quite lower than values reported in literature [10]. Here, it is

Table 2. Active Raman modes and direct band gap energies (E_g) for ZCA, ZCA450 and ZCA700 NPs.

Sample	Positions of Raman modes in cm^{-1}			Maxima of absorption		E_g ±2 (eV)
	$2E_{2H}$-$2E_{2L}$	E_2 (high)	E_1 (LO)	λ (nm)	E (ev)	
ZCA	-	-	-	376	3.30	2.74
ZCA450	346.5	438.1	582.6	378	3.28	2.50
ZCA700	331.7	439.6	583.8	377	3.29	2.68

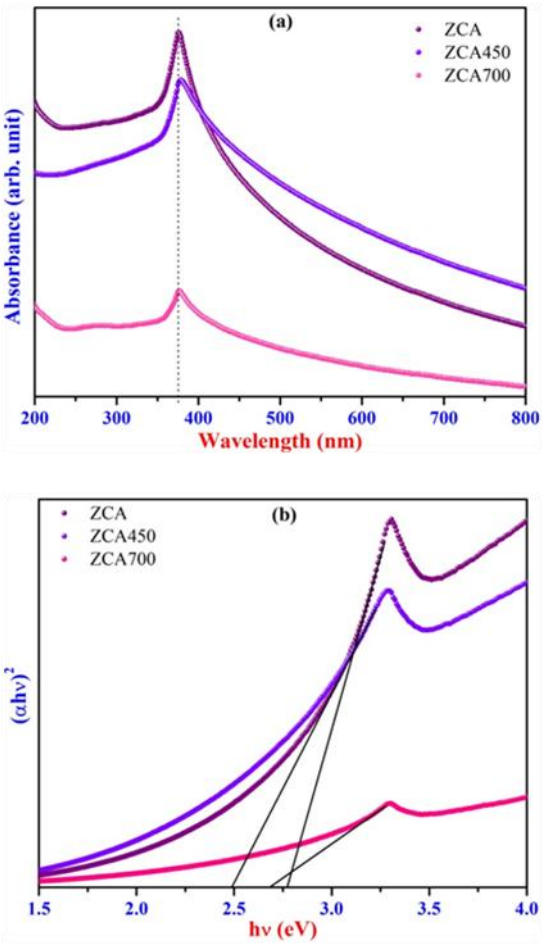

Figure 6: (a) UV-VIS-NIR optical absorption spectrums and (b) Tauc's plots for ZCA, ZCA450 and ZCA700 NPs.

worth to note that below 500 nm, these ZnO NPs considerably absorbed light and the maxima is noted in the blue region. These outcomes could be useful for making UV & blue light protection layer and absorber for sunscreen lotion etc.

ESR is a unique technique for identifying defect centers like oxygen vacancies (V_o) and cationic vacancies (V_{Zn}) in metal oxide nanoparticles, which greatly affect their optical properties. ESR spectra of ZCA, ZCA450, and ZCA700 NPs are shown in Figure 7. The resonance field (H_{res}), g-factor, and peak width (ΔH_{pp}) values are listed in Table 3 [7]. In these ZnO NPs two prominent ESR signals are detected at g ~2.00 (S_1) and g ~1.96 (S_2).

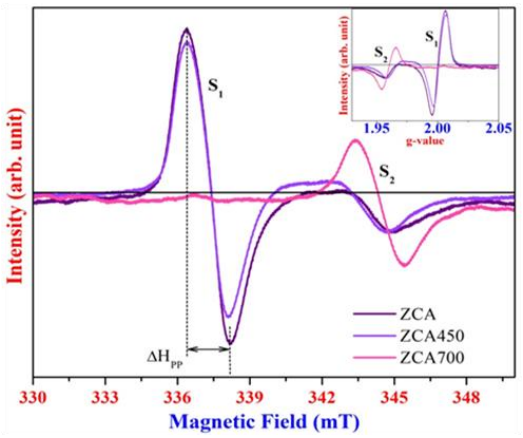

Figure 7: ESR spectrums of ZCA, ZCA450 and ZCA700 NPs.

In bulk ZnO only the S_2 signal has been reported in the literature. The S_1 signal is related to surface oxygen (V_o) defects and their concentration decreases with annealing temperature, indicating reduction in the defects at higher temperature. There is a debate on the origin of S_2 signal, some reports attributing it to V_o, hydrogen defects, or shallow impurities [3]. While other studies have suggested that S_2 signal is originated due to Zn vacancies (V_{Zn}), instead of V_o, with V_{Zn} in various charge states like V_{Zn}- can distorts the lattice and creates paramagnetic O^- defects (g ~1.96) [13]. Increasing AT raises in content of V_{Zn}- as depicted by a stronger S_2 signal; these findings are aligning well with recent defect studies on ZnO NPs [14]. In summary, annealing significantly impacts defect formation in ZnO lattice, with V_o promoting reactive oxygen species (ROS), which are useful in waste water treatment and other environmental remediation and thus, highlighting potential of ZnO NPs in future R&D activities.

Table 3: Resonance field, g factor and peak width of ZCA, ZCA450 NPs

Samples	H_{res}	(ΔH_{pp})	g-value	
			S_1	S_2
ZCA	337.41	1.86	2.00028	1.9671
ZCA450	337.39	1.73	2.00095	1.9670
ZCA700	344.31	2.05	-	1.9607

Conclusion

Phase pure samples of ZnO NPs (ZCA, ZCA450 & ZCA700) were successfully synthesized by sol-gel auto combustion reactions. XRD and Raman analysis revealed that the prepared ZnO NPs crystallize in the single-phase

Wurtzite type hexagonal structure. Monotonic increment in the unit cell parameters 'a' and mean crystallite size 'D' with annealing temperature is observed. Blue shifting in the Raman E_2 (high) and E_1 (LO) vibration modes and red shifting in the $2E_{2H}$-$2E_{2L}$ mode with annealing temperature and ESR analysis affirmed formation and annihilation of surface defects with increasing annealing temperature in ZnO NPs. Below, 500 nm these ZnO NPs considerably absorb light with a maximum noted in the blue region. Band gap energy of ZnO NPs decreases with annealing. These ZnO NPs seems to be useful for making UV & blue light protection layers and UV absorbers for sunscreen lotion etc.

References

1. J. Chen, Z. Tang, Y. Zhou, T. Zhang, L. Qian, C. Xiang, Chem. Phys. Lett. (2023) 140441.
2. S. Zeghoud, H. Hemmami, B. Ben Seghir, I. Ben Amor, I. Kouadri, A. Rebiai, M. Messaoudi, S. Ahmed, P. Pohl, J. Simal-Gandara, Mater. Today Commun. 33 (2022) 104747.
3. V. Ischenko, D.G. Polarz, V. Stavarache, K. Fink and M. Driess, Adv Funct Mater 15 (2005) 1945–1954.
4. K. Punia, G. Lal, P. Alvi, S.N. Dolia, S. Dalela, K.B. Modi, S. Kumar, Cerams. Int. 45 (2019) 13472–13483.
5. H. Bhoi, P. Joshi, K. Punia, G. Lal, S. Kumar, AIP Conf. Proc. 2220 (2020) 020109.
6. H. Bhoi, K. Punia, G. Lal, S. Kumar, AIP Conf. Proc. 2265 (2020) 030117.
7. K. Punia, G. Lal, H. Bhoi, S. Kumar, AIP Conf. Proc. 2115 (2019) 030146.
8. J. Ungula, B.F. Dejene, H.C. Swart, Results Phys. 7 (2017) 2022–2027.
9. H. Bhoi, S. Tiwari, G. Lal, K.K. Jani, S.K. Modi, P. Seal, V. Saharan, K.B. Modi, J. Borah, K. Punia, S. Kumar, Ceram. Int. 48 (2022) 28355–28373.
10. K. Punia, G. Lal, S.K. Barbar, S.N. Dolia, P.A. Alvi, S. Dalela, S. Kumar, Vacuum 184 (2021) 109921.
11. J. Lv, M. Fang, Mater. Lett. 218 (2018) 18–21.
12. H. Bhoi, S. Tiwari, Manisha, Hirdesh, L. Pascual, S. Kumar, Inorg. Chem. Commun. 170 (2024) 113487.
13. N. Y. Garces, L. Wang, L. Bai, N. C. Giles, L. E. Halliburton, G. Cantwell, Appl Phys. Lett. 81 (2002) 622.
14. S. Nadupalli, S. Repp, S. Weber, E. Erdem, Nanoscale 13 (2021) 9160–9171.